Composites: Part A 84 (2016) 175–185

Contents lists available at ScienceDirect

Composites: Part A

journal homepage: www.elsevier.com/locate/compositesa

Novel method for functionalising and patterning textile composites: Liquid resin print

Dmitry S. Ivanov [a,*], Yann M. Le Cahain [a], Surush Arafati [a], Alexandre Dattin [a], Sergey G. Ivanov [b], Andrey Aniskevich [b]

[a] Advanced Composites Centre for Innovation and Science, University of Bristol, Queen's Building, University Walk, Bristol BS8 1TR, United Kingdom
[b] Institute of Polymer Mechanics, University of Latvia, 23 Aizkraukles Str., Riga LV-1006, Latvia

ARTICLE INFO

Article history:
Received 14 September 2015
Received in revised form 4 January 2016
Accepted 23 January 2016
Available online 3 February 2016

Keywords:
A. Carbon nanotubes and nanofibers
A. Multifunctional composites
B. Electrical properties
E. 3-D printing

ABSTRACT

The paper reports a novel method of integrating resin into continuous textile reinforcement. The method presents a print of liquid reactive resin into textile preforms. A series of targeted injections forms a patch which upon consolidation and curing transforms into a stiff region continuously spanning through preform thickness. Enhancing the injected resin with conductive phase allows creating a pattern of patches with controlled dimensions and added functionalities. Patterned composites reveal features which are not typical for conventional composites such as fibre bridged interfaces, regular thickness variation, and gradient matrix properties. The presented study explores the role of these features in (a) the mechanical behaviour of these materials, focusing on their deformation and failure mechanisms in tension, and (b) the feasibility of adding functionality by printing electrically conductive resins containing carbon nano-tubes (CNT). It was shown that resin print is a promising method for local functionalization of structural composites.

1. Introduction

The study investigates potential of a novel manufacturing method that can create local patches or pins of matrix spanning through the thickness of a continuous textile preform. The method of liquid resin print was originally developed for stabilising textile preform prior to the infusion [1]. It allows creating a stiff skeleton within a compliant preform which secures the material in a predefined shape through the infusion and consolidation stages. The process is implemented by injecting liquid reactive resin using a syringe with a needle inserted to a predefined depth into textile preform. Each injection creates a thin layer of liquid resin in the plane of preform. The resin flow around the needle tip occurs predominantly due to the capillary forces and lower in-plane permeability compared to the through-thickness permeability. A series of injections through-thickness connect these layers and, upon heat and pressure assisted consolidation, a solid patch is formed. The dimensions of the patch can be controlled through the volume of each injection. In addition, the bespoke printer allows creating patches arranged in any programmed pattern and density.

Thus, the method is implemented in the spirit of additive manufacture. However, unlike the conventional 3D print process, the deposited resins are liquid and reactive. Printing liquid resin is possible due to the intrinsic architecture of textile medium which allows distributing the resin around the injection point and holding the fluid in place until the material is fully consolidated. The liquid state of the deposited resin gives other advantages. For example, as will be shown further in this paper, it easily allows introducing additives to the injected resin systems and tuning local material properties.

The ability of incorporating additives locally makes the process attractive for functionalization. The composites community has been consistently targeting at increasing efficiency of composites by enhancing structural composites with thermal, electrical, damping and other properties. Even though many different methods were recently developed to incorporate function-carrier additives into material there is still a challenge of creating functional reinforcements locally, precisely where needed and without introducing a major impact on the manufacturing process, internal architecture and structural composite properties.

The resin print process allows addressing some of these challenges integrally. After the local patches are created where required, any conventional liquid moulding process can be applied to create a composite component. Away from the patches the

* Corresponding author.
E-mail address: Dmitry.ivanov@bristol.ac.uk (D.S. Ivanov).
URL: http://www.bristol.ac.uk/composites/ (D.S. Ivanov).

http://dx.doi.org/10.1016/j.compositesa.2016.01.018
1359-835X/

reinforcement geometry remains unaffected and so overall the process complies with requirement of being minimally invasive. However, patching does create a number of unconventional structural features in the modified area whose impact on composite performance needs to be studied:

(1) *Fibre bridged interfaces between printed and infused zones:* since the patches are cured prior to infusion a weak interface between matrices of the cured and infused regions can be expected. Unlike other known and well-studied interfaces (e.g. fibre-to-matrix, ply-to-ply, grain-to-grain), patch interfaces are bridged by fibres and conduct the load normal to its boundaries. These interfaces present a particular interest in the context of damage accumulation process and their role is not yet known.
(2) *Thickness variation:* the patches are consolidated at a higher pressure level than used for resin infusion process under flexible bagging. This is needed to suppress voids resulting from the unsaturated capillary flow. As a result the composite thickness may (or may not depending on a reinforcement and preform type) be lower in the patched region. This creates a wavy surface and an additional fibre crimp that may negatively affect composite strength.
(3) *Varying matrix properties:* the interaction of various matrices with distinctly different properties affects stress distribution and load flow. It can be expected that this factor may play a role in damage accumulation process.

If the patch pattern is regular, these features introduce a new material scale intermediate between the component scale and characteristic scale of textile unit cell. At this scale the architecture is fully defined by the settings of the injection printer and can be adjusted to reach an optimum composite performance. The first step towards the optimisation is to understand how these features affect strain distribution and failure behaviour of the material. The paper reports an experimental characterisation of the patched patterned composites using tensile tests with in-situ measurements of local strain evolution and post-mortem characterisation of damage and failure.

The second challenge addressed here is to understand the potential for functionalization. The focus of this work is on through-thickness electrical conductivity. This property is critically important for lightning strike protection and release of static charge. Electrically conductive composites have also a potential for damage and strain sensing [2,3]. The commonly adopted approach for enhancing this property is to incorporate third phase into a composite: conductive particles. Carbon nano-tubes (CNT) tend to be particularly attractive as their high aspect ratio helps forming a percolation network at very low weight fractions. Among recent developments targeted specifically at improving conductivity there are methods such as growing CNT grown on fibre surfaces [4,5], integrating CNT in fibre coating or sizing [6,7], depositing CNT in powder form on fibre surface [8,9], and delivering CNT within the resin in a liquid moulding process [10–14]. These studies show that material can acquire electrical conductivity if percolation of CNT is achieved. Providing electrical percolation through the thickness of glass composites is most challenging since the formation of CNT networks is impeded by non-aligned non-conductive fibres [14].

Most of the known methods require significant changes to manufacturing process to enable functionalization. For instance it is known that growing CNT on fibre surfaces may impact on fibre strength and compressibility of the preform [15], resin infusion may be impacted by the high viscosity of CNT solution and filtration mechanisms [19]. The formation of agglomerates and re-agglomeration during mixing, cure and consolidation processes [11,16] significantly limits the weight fraction of CNT realistically achievable for RTM process. da Costa et al. [11] found that the suspensions of CNT with loading above 0.5 wt.% were not appropriate for liquid moulding.

This paper aims to demonstrate that CNT can be incorporated in a radically new way. Liquid resin print may present a remedy for some of these problems by delivering required amount of CNT fraction precisely where needed without affecting the subsequent infusion process. This studied process has a potential to eliminate the issues associated with large flow lengths. The resin is deposited locally, point wise and hence, much higher volume fraction can be allowed. Mechanical testing was then used to assess how structural properties were affected by the new process.

2. Materials and composites manufacturing

Patterned samples were manufactured using a two-step manufacturing technique. In the first step, the reactive liquid resin containing dispersed CNT was printed into a dry multi-ply textile laminate. The print procedure was followed by curing and consolidation in a hot press to create cured patches. In the second step the material was infused using a variant of vacuum assisted Resin Infusion with Flexible Tooling (RIFT) with a conventional epoxy system. The composites with integrated CNT patches were compared with a reference composites obtained by RIFT alone. Carbon Five Harness Satin (5HS) and Glass Mock Leno (ML) woven composites were chosen as representative woven fabrics. For 5HS composites an extra configuration was considered: patterned with pure epoxy. This allowed distinguishing evolutions of conductivity of carbon fabric associated with consolidation and fibre fraction evolution from the added effect of CNT presence. This made five material configurations: (1) 5HS-I: reference composite infused using RIFT, (2) 5HS-P: with a pattern of patches printed using the same resin as for the subsequent RIFT, (3) 5HS-CNT: carbon composite with a pattern of CNT-enhanced resin, (4) ML-I: the reference glass composite infused using RIFT, (5) ML-CNT: glass composite with CNT-enhanced resin patches.

2.1. Materials

Two types of reinforcement were used in this study:

(1) Carbon woven 5-harness satin (5HS) fabric (Mouldlife A0277/000, with an areal density of 285 g/m^2 per ply, 3 K yarns and a yarn spacing of 1.43 mm, Toray T300B fibres), the preforms were constructed of 18 plies laid-up in the warp direction.
(2) E-glass woven Mock Leno (ML) fabric (Hexcel HexForce 00695) with yarn spacing ranging from 1.2 mm to 2.4 mm, areal density 223 g/m^2. The fabric is sparse and has large inter-yarn openings of approximately 1.2 by 1.2 mm size. The glass preforms were constructed of 14 plies to have a comparable thickness with carbon samples.

The patterns of these fabrics, produced by WiseTex software [17], are shown in Fig. 2.

Baseline matrix system used for the infusion and printing was Prime 20 (by Gurit) – low viscosity system specifically designed for liquid moulding process. The resin was degassed for 4 h prior to mixing with hardener and around 20 min after it was mixed. The CNT enhanced resin was prepared using Nanocyl master batch Epocyl NC R128-02 (3% CNT weight fraction as suggested by Korayem et al. [18]), which was based on Bisphenol-A resin. The resin was diluted in the ratio 1:2, which exceeded the ratio recommended by manufacturer by a factor of three. As a carrier, Araldite

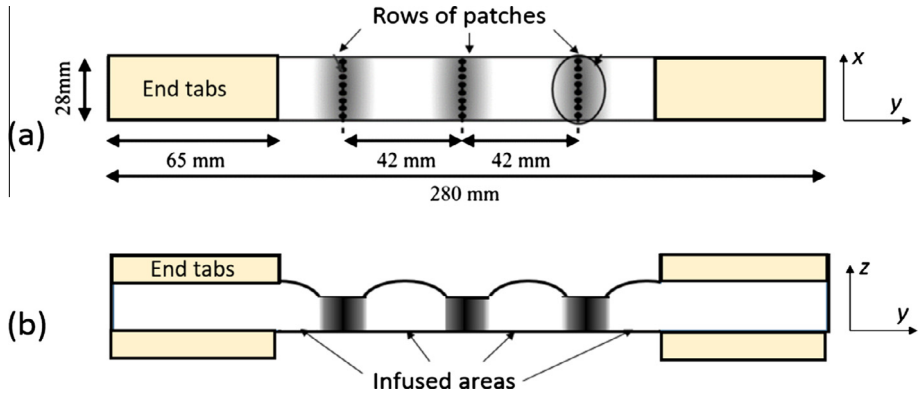

Fig. 1. Dimensions and print patterns of specimen for tensile tests: (a) in-plane, (b) out-of plane (thickness variation in *y*–*z* plane is due to the difference in consolidation pressure in infusion and injection processes). (For interpretation of the references to colour in this figure legend, the reader is referred to the web version of this article.)

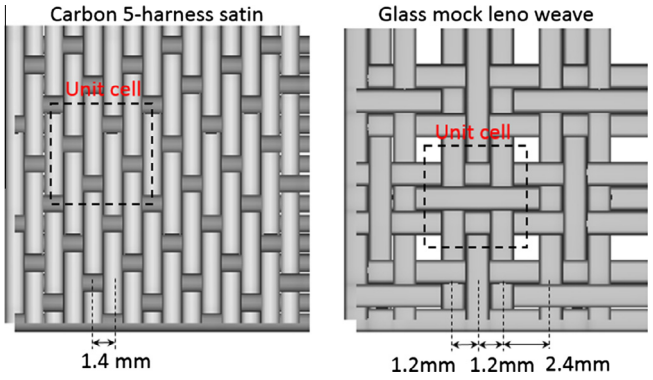

Fig. 2. Architecture of two fabrics used in the study. The models are produced by WiseTex software [17]. (For interpretation of the references to colour in this figure legend, the reader is referred to the web version of this article.)

LY 1564 resin with Hardener XB 3486 produced by Huntsman were used. The CNT dispersion procedure was arranged as follows: (a) mixing the resin with master batch in a high shear mixer Silverson L5M for 13 min at 3500 rpm, (b) pulse sonication (using high intensity VCX-750 Sonicator) of the obtained solution with 5 s on/3 s off programme for 15 min and inputting energy of 852 J/g, (c) the resin was then degassed for 1 h, (d) the degassed resin was then mixed with hardener and, finally, (d) degassed for another 15 min before being injected. In general, this mixing procedure is common in the context of liquid moulding procedures and allows achieving an acceptable level of CNT dispersion.

2.2. Injection procedure

The print process was realised by means of a novel liquid resin print rig. It was built by modifying the RepRap Mendel 3D printer [1] where a thermoplastic extruder was substituted by a syringe holder (standard medical 10 ml syringes could be fitted, 21G needles with an outer diameter of 0.8 mm and inner diameter of 0.5 mm were used in this study). The printer has three translational degrees of freedom to move the syringe's needle and an independent controller enabling the injection of the specified amount of resin at a required speed and quantity. The rig is capable of implementing programmed injections in any position both in-plane and through-thickness of a preform. The injection speed was set to be 2 ml/min. The pause time, set after every injection to let the resin flow, was 3.5 s.

The number of injections per thickness was chosen to have at least one injection per ply, i.e. 19 injections for 18-ply carbon preform and the same number of injections in the glass preform with fewer plies. The step between injections was chosen based on a bespoke measurement of preform thickness using the injection rig. To do that the needle was inserted all the way through the preform down to the tool side and then incrementally taken out with a fixed step until the needle tip could be seen. The needles were significantly tapered – 3 mm long which helped to minimise the damage to the fibres when inserting the needles but created a difficulty in impregnating the bottom ply. To avoid a non-uniform impregnation, the preform was placed on a soft silicon pad and the needle at its lowest position was inserted half-way through the taper into the silicon. The preforms were wrapped in a loose film and constrained by the tape to avoid unintentional movement when the preform was moved from the printer to the press where the patches were consolidated. This film did not aim at mitigating against preform deformation during consolidation and infusion. After the patches were cured the preform did not require any further constraining and presented integral interconnected material which could not be disintegrated or change dimensions in the following manufacturing processes. In a prospective print process film wrapping will not be necessary if the preform is consolidated in-situ. Rectangular 125 × 300 mm preforms were used for most of the injection and infusion procedures which in general allowed producing three tensile samples out of each plate.

The need to study the role of the interface dictated the simplest print pattern – two/three rows of patches were printed across the sample width – Fig. 1. Patches within the row were placed sufficiently close to be merged and form a continuously printed rib so that the loading in the tensile test is normal to the interface of the rib. The parameters of the injections, patches and pattern are given in Table 1. All the CNT-patterned samples were produced

Table 1
Parameters of injection programme.

Parameters of each injection Programme A/Programme B		Parameters of patch Programme A/Programme B		Parameters of pattern Programme A/Programme B	
Injection step in through-thickness direction, mm	0.7	Distance between patches in a row, mm	7	Distance between the rows, mm	42
Number of injections per thickness	19	Number of injections in a row	15	Number of rows	2/3
Resin volume per injection, μl	8/6	Total injected volume per patch, μl	152/114	Row width/patch diameter, mm	24/18
Pause time after the injection, s	3.5				

using the programme A. For the only non-CNT patterned configuration (5HS-P) a slightly different programme (B) was applied, which resulted in a larger patch size. This programme was implemented for technical reasons but not to study the effect of injected volume on the mechanical performance.

The printing process was followed by a consolidation procedure, targeted at curing the patches and suppressing porosity. Since the injection flow is not vacuum assisted and driven by a relatively small pressure gradient, the flow was highly unsaturated and entrapped a noticeable fraction of voids behind the flow front. Upon applying pressure these voids tended to form micro intra-yarn porosity in dense fabrics and large inter-tow pores in open fabrics with large intra-yarn spacing. A consolidation procedure was set to improve the quality of the patches. The preform with injected patches was heated in oven at 60 °C for 30 min prior to application of the consolidation pressure. This transformed the matrix to a state where it gelled but was not fully cured. In a follow-up compaction the high viscosity of resin reduced the flow lengths and prevented squeezing the resin out of the patch boundaries. Instead, the resin carried the major fraction of applied pressure which was sufficient to suppress the voids in the patch centre. In the current version of the process all the patches were cured and consolidated at once in a hot press with pressure exceeding 6 bar applied for 5 h at 60 °C. For an industrial environment, it would be possible to modify the process by adopting fast curing resins and applying local tooling for consolidation to make consolidation almost instantaneous but this discussion goes beyond the scope of the paper.

2.3. Infusion procedure

The patterned rectangular preforms were impregnated in a resin infusion process with flexible bagging. The rectangular preforms were infused across their long sides. The injection port was placed outside the preform delivering resin directly to a distribution spring oriented along the preform. The distribution mesh was placed on the top and bottom of the composite preform conducting the resin in the width direction. Another spring was placed parallel to the first one on the other side of the preform to collect the propagated resin. A uniform flow front was achieved and the infusion was completed in roughly 20 min. Infused part was then cured in the oven at 50 °C in 16 h in line with the specification of resin manufacturer. The same resin infusion procedure was applied to the reference and patterned samples.

2.4. Features of patterned composite

The micrography and dimensional assessment of patterned panels revealed the following features:

(1) *Thickness variation* in the carbon preform between the patches (consolidated at high pressure) and the infused area (consolidated under vacuum bag) varies by roughly 15–20% – Table 2. The bottom surface, which was in contact with the tool, was flat while the top surface has acquired three (or two in the case of CNT patching) waves of a regular undulation – Fig. 1b. In the glass ML preform the thickness variation between the infused and printed patches was considerably lower due to the higher nesting of the plies and a weaker spring-back reaction of preform after consolidation.

(2) *Impregnation quality and patch interfaces.* On sample surface, the rows of patches formed well-defined regions of rectangular shape spanning across the samples width with darker sub-domains showing regions with higher fraction of CNT resin – Fig. 3b and c.

In the patch regions a distributed micro-porosity was seen. Few larger isolated pores with a characteristic size under 0.2 mm could be found in the central infused area. The maximum porosity was found on the boundary between infused and printed region with a relatively good impregnation close to injection sites. The primary reason for the micro pore occurrence was the air entrapment behind non-uniform flow front occurring due to the dual scale flow. The consolidation procedure described above in Section 2.2 was aimed at suppressing the voids using compaction of nearly gelled resin. This did help to improve the impregnation quality in the centre of the patch but could not fully suppress defects on the patch edges: pressure in resin inevitably decays at the patch boundaries.

Compared to pure epoxy patches the CNT patches revealed higher level of micro-porosity and occasionally the presence of bigger inter-yarn impregnation defects – Fig. 4. This feature was likely caused by sonication of CNT resin and subsequent degassing which struggled to eliminate all the voids. Apart from the non-uniformity of micro-pores no visible interface between the printed and infused regions could be seen – Fig. 5b. It can be suggested that the interface presented a finite volume where injected and infused resins shared a finite space rather than a 2D boundary between the distinctly different regions.

(3) *Filtering of CNT:* Relatively high fraction of the CNT-enhanced resin led to a clearly observed filtering mechanism. The darker coloured region (containing CNT) appeared to be approximately twice as small compared to the overall patch size both in glass and carbon preforms – Fig. 3. This implies that the content of the CNT in the close vicinity of injection is higher compared to the CNT content of injected resin. On the one hand, the length of CNT propagation (~8 mm for 5HS and ~13 mm for ML) could be attributed fabric architecture. The CNT flow length as comparable to the dimensions of unit repeats of textiles, which is 6.9 mm for carbon 5HS and 4.8 mm for glass ML samples. On the other hand, the flow length characterises the dispersion quality. Fan et al. [19], suggested an experiment where a glass yarn was immersed in a CNT solution. They found that depending on dispersion quality the length for CNT propagation varied between 2 mm (large agglomerates) and 20 mm (fine dispersion).

In the settings of a conventional liquid moulding process high degree of filtering would be unsatisfactory for the process and would be evidence for insufficient dispersion of the CNT in the

Table 2
Thickness of patterned and infused samples.

Samples	5HS-I carbon infused	5HS-P carbon patterned without CNT	5HS-CNT carbon patterned with CNT	ML-I glass infused	ML-CNT[a] glass patterned with CNT
Patch region, mm	n/a	4.6 ± 0.2	4.6 ± 0.1	n/a	4.2 ± 0.2
Infused area, mm	5.3 ± 0.2	5.5 ± 0.3	5.3 ± 0.1	5.1 ± 0.1	4.8 ± 0.1

[a] The provided data for ML-CNT are measured after polishing the patch area.

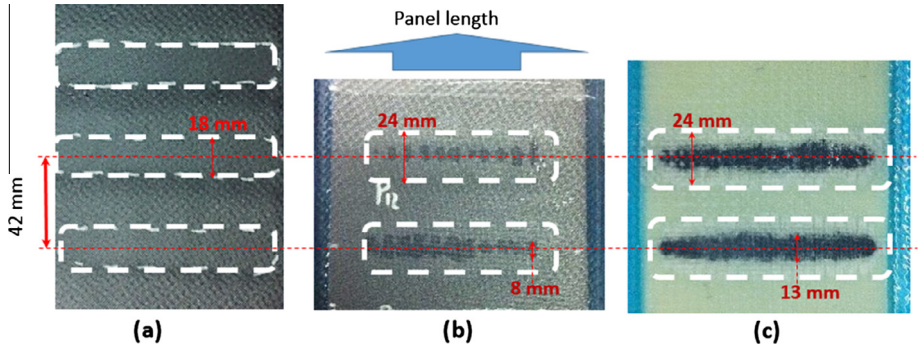

Fig. 3. Rows of patches: (a) Prime 20 resin injected into carbon 5HS preform (Programme A), (b) CNT enhanced resin injected into carbon 5HS preform (Programme B), (c) CNT enhanced resin injected into glass Mock Leno preform (Programme B). White dash contours show the visible external boundaries of the patch row. Darker areas in figures (b) and (c) reveal the CNT rich regions. (For interpretation of the references to colour in this figure legend, the reader is referred to the web version of this article.)

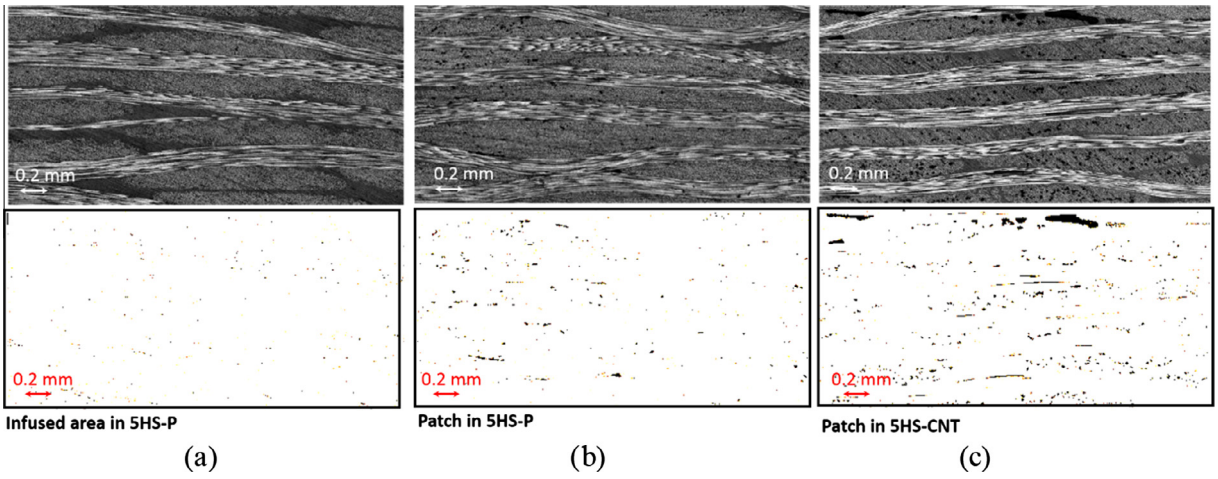

Fig. 4. Three representative micrographs: (a) Infused area in patterned 5HS-CNT samples (similar micrographs are seen in 5HS-I and in the infused area of 5HS-P), (b) patch areas in composite patterned with Prime 20 resin (5HS-P), (c): patch areas in composite patterned with CNT-enhanced resin (5HS-CNT). Figures below show the same images with a different contrasts setting to highlight the porosity distribution. (For interpretation of the references to colour in this figure legend, the reader is referred to the web version of this article.)

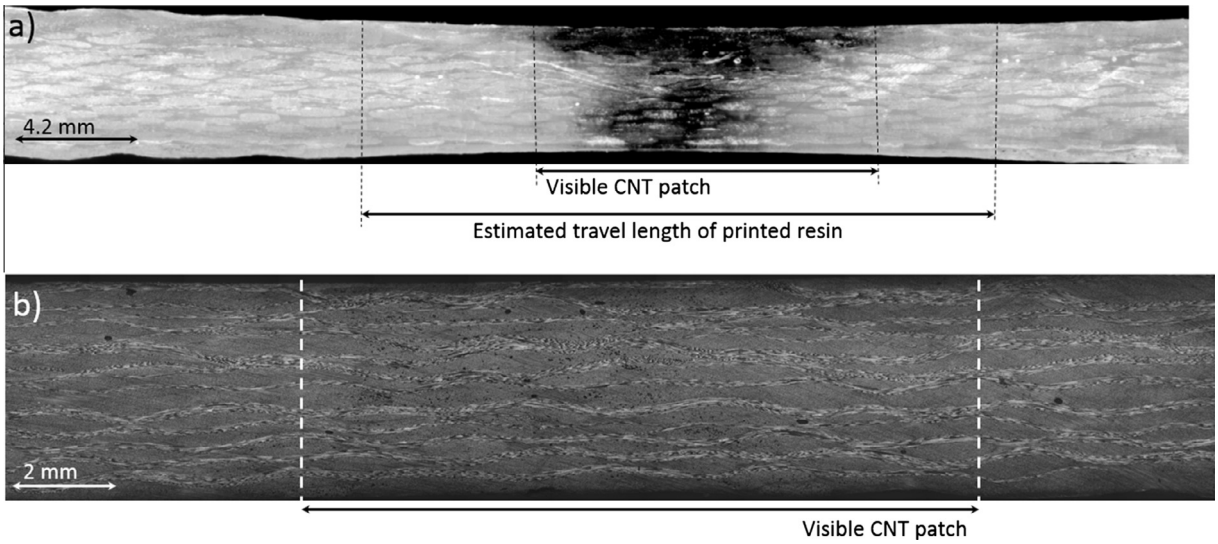

Fig. 5. CNT patch in a ML glass preform: (a) Scan of 1.3 mm slice cut in the local proximity of the needle insertion, (b) micrograph of the correspondent CNT patch.

solution. In the resin print process, the higher loading may be beneficial for the local conductivity and creating a higher contrast in local material properties. A scan of a thin glass composite slice made in the vicinity of the injection, Fig. 5, revealed that CNT tended to fill inter-yarn space sometimes enveloping the yarns. It also showed a non-uniform distribution of injected resin through

Table 3
Conductivity of patterned samples and injected resins.

Fibres	T300B carbon		T300B carbon		E glass		No fibres	
Material	5HS-CNT (Batch 1)		5HS-P		ML-CNT (Batch 2)		CNT-epoxy resin (from syringes)	
Location	Row 1	Row 2	Row 1	Row 2	Row 1	Row 2	Batch 1	Batch 2
Thickness, mm	4.41	4.50	4.45	4.45	4.21	4.07	13.6	12.7
Resistance, Ω	2.1	2.5	2.6	2.1	$14.7 \cdot 10^3$	$15.1 \cdot 10^3$	$175 \cdot 10^3$	$8300 \cdot 10^3$
Conductivity, S/m	74.31	63.69	61.79	74.98	0.0101	0.0095	0.0027	0.0001

thickness which implied that the local inter-connectivity between the layer of liquid resin could be further improved by increasing the number of injections through thickness. The filtering was much more intensive in the carbon samples which may be explained by the fact that it had significantly smaller inter-yarn space and inter-bundle channels.

2.5. Samples for tensile testing

Glass woven EF1612 prepreg was used for end-tabs. The 8-ply stack was cured in an oven at 130 °C for 15 min in line with the specification of the manufacturer. The resultant thickness was 1.9 mm. The end tabs were glued to each panel and then cured at 80 °C for 2 h and then cut to 3 tensile test samples of 28 mm in width. The sample edges were polished to remove any defects possibly imposed by the diamond saw. At least three samples were prepared for all five materials configurations considered in the study.

3. Testing of patterned composites

3.1. Conductivity measurements

In order to measure the conductivity the surface in the location of measurements (in the patch region) was slightly polished. This was required to eliminate a thin insulating layer of resin created during post-printing infusion and covering the patch surface; the conductivity was beyond the sensitivity of measuring device when this operation was not performed. Thickness measurements conducted on selected samples showed that polishing removed about 50 μm on each side. The authors believe that this was mostly a surface layer of resin left by the distribution mesh. Some fibres at surface could be affected by polishing but their fraction would be low to have any pronounced impact on the mechanical properties due to the considerable thickness of the laminates.

Once polished the surface was cleaned and a thin layer of conductive silver-based glue (L100 from Kemo Electronic) was applied on top and bottom sides of patched region to improve the contact between the electrodes and the composite surface. The diameter of the conductive spot was chosen to be 6 mm as it was comparable then to a characteristic CNT rich zone within the patch. The resistance was measured using a multimeter tester UNI-T UT33D and the conductivity was calculated by reversing the resistivity value and taking into account the spot area and the local composite thickness in the studied location. The conductivity was also measured in the syringes where resin remained after the injections. The cylindrical samples of CNT resin cured after injections at room temperature were cut from syringes to measure their conductivity. The top and bottom surfaces were polished and the conductive silver glue spots of the same dimensions as for the composite samples were applied on flat surfaces. The results are shown in Table 3.

The through-thickness conductivity of the carbon samples with no CNT was high and the presence of CNT patches did not affect the resistance. The obtained values were comparable but somewhat higher than measured for flat laminates [20], which can be explained by higher alignment of crimped textile yarns with the measurement direction. The electrical conductivity of the reference non-functionalised glass samples was beyond the sensitivity of the tester and can be considered practically non-conductive. The conductivity was significantly improved through adding CNT.

Their absolute values were still significantly lower than that of the carbon composite. However, they were significantly (1–6 orders of magnitude) higher than the values previously reported elsewhere for CNT enhanced glass composites obtained with liquid moulding technologies [10–12] and comparable to the conductivity of the glass composite with CNT grown on fibre surface [5]. Comparing the through-thickness properties of glass composites to the correspondent value for the injected resin gave an insight on the reason for this unusually high performance. Against obvious expectations, the conductivity of glass composite appeared to be considerably higher – Table 3. The increase in conductivity was most likely related to the intensive filtering of carbon nano-tubes around the injection spot as evidenced by Figs. 3c and 5a. Filtering left much higher fraction of the CNT in the vicinity of the location where conductivity was measured. Apart from this direct optical observations it is suggested that the other factors could play a role as well:

(1) The orientation of the CNT by the resin flow in the needle helped to align the CNT in the thickness direction, and created a better percolation network compared to the reference resin sample where CNT orientation was random. A positive role of CNT orientation is known from the studies where alignment of nano reinforcement was implemented using electric or magnetic fields [21–23].
(2) The resin in glass composite was compacted after gelling which could well lead to a squeezing flow and, as a result, to reconfiguration and merging of the CNT clusters whereas the resin in syringes was cured in oven without any pressure imposed.
(3) The needle insertion left traces in the preforms: thin channels comparable in dimensions of the needle – 0.5 mm [1]. This could further increase the probability of forming a continuous network in the through-thickness direction.

3.2. Mechanical testing of patterned composites

The tensile tests were performed on a 250 kN Instron hydraulic machine. La Vision 3D Digital Image Correlation (DIC) system was used to assess the difference in strain distribution due to the variation in thickness and fibre volume fraction and measure the applied strain field calculated as an average strain over the sample surface. The flat sample sides were speckled by black spray on uniformly painted white background. The field view covered the area of ~512 pixels (28.0 mm) along the sample width and ~2010 pixels (110 mm) along the length. The characteristic speckle size was around 0.5 mm. The displacement was determined on the subset size of 17 pixels (equivalent to 0.9 mm) and the step between the subset was chosen to be 8 pixels (equivalent to 0.4 mm).

The strains were measured both in the smooth patch and rough infused areas. The deformation of rough surface could contribute to the noise however, the use of stereo strain measurements helped to eliminate the impact of the out of plane roughness on the measured signal.

In further discussion the results of the tensile tests are shown in load–strain diagrams as opposed to traditional stress–strain presentation of test results. This was more appropriate when comparing samples with thickness variation and where the load normalized by cross-section area differed along the sample length. It is important to note that the amount of fibres in any cross-section along the length of the sample was the same in all the compared patterned vs. reference samples.

3.2.1. Carbon composites

The carbon samples exhibited a linear load–strain response till failure. Failure of the reference infused 5HS samples occurred in the grips at applied strain in the range of 1.1–1.2%. The patterned samples ruptured predominantly in the patterned area (6 out of 8) with few samples failing in the interface region (2 out of 8 samples). Incorporation of the CNT did not seem to have a massive impact on damage mode or load/strain at failure – Fig. 6. However, there was a slight increase in average strain at failure – Table 4. The failure mode in all the cases was brittle and the fibre rupture zone was localised in a 5–10 mm zone showing traces of highly localised delaminations around the fracture (possibly occurring after the initial fibre rupture).

The surface strain measurements revealed three distinctly different regions in the patterned samples: the infused region, the patched region and an interface between them – Fig. 7a. The highest strain, averaged over the examined region, was observed in the infused area and the lowest at the patch interfaces. The strain variation was pronounced – at failure the average strain in the infused region reached 1.2% whereas at the interfaces the strain hardly exceeded 0.8% reaching 40% difference. The average strain at failure in the patched region was 0.9–1.0%. Despite the high strain contrast, the failure location did not correlate with the location of maximum strain often occurring in the region of lower strain. Hence, in this case the strain in the damaged region could not be used as an indicator of failure risk.

The infused region exhibited a much higher gradient of local strain clearly revealing the textile pattern, whereas strain in the patched region was much more uniform. This can be explained by the fact that the infusion process where the preform, being constrained by a flexible bagging, left a textile imprint on the composite surface, whereas the patterned region, consolidated under the press, tended to be much smoother. In addition to that the patch areas were slightly polished to remove the thin surface layer of resin for measuring conductivity.

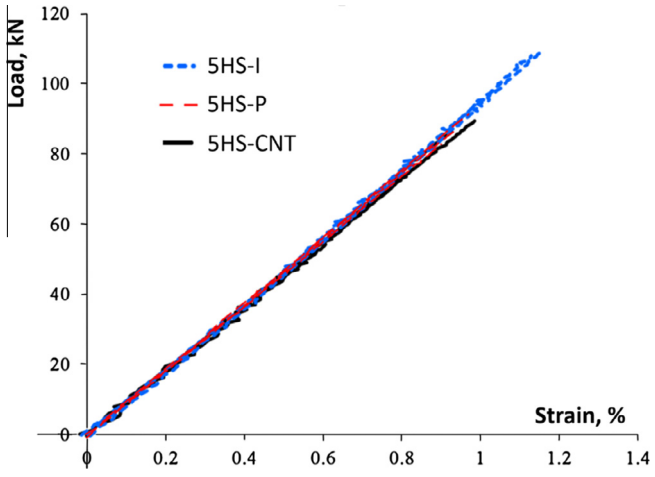

Fig. 6. Mechanical response of the patterned 5HS-P and 5HS-CNT (failed in patch region) and reference/infused 5HS-I samples (failed in the grips). (For interpretation of the references to colour in this figure legend, the reader is referred to the web version of this article.)

The high variation of strain over the infused-printed areas is likely to be caused by the thickness variation which created additional local bending effects superimposed with the applied tension. Local strain in 90° weft yarn at failure load approached 1.7%. However, the average strain response in all the three regions appeared to be linear till failure for the case when patched and infused resin was the same. In CNT-enhanced patches at ~0.8% a non-linearity in the interface region and small but visible kinks were observed in the infused and patched zones, Fig. 7b, pointing at a damage event.

To investigate the residual deformations indicating irreversible deformations or damage, several samples were loaded till 77 kN (90% of the apparent strength of the samples) and then unloaded at 1.5 mm/min while tracking the surface strain evolution. The residual strains, most likely localised in the 90 yarns, reached the value of 0.3% compared to the reference state prior to testing.

3.2.2. Glass composites

The glass samples revealed a non-linear response related to intensive damage accumulation. Deviation from linear response started at approximately 0.25% of applied strain – Fig. 8a. The initial stiffness and the strain at the kink are the same for reference infused ML-I and patterned ML-CNT samples. The secant stiffness after the kink was slightly lower for the patterned samples pointing at higher intensity of damage events in the patterned sample. Both the sample types experienced the onset of fibre rupture at approximately the same applied strain level (1.23% for ML-I and 1.17% ML-CNT) but load at this drop is slightly higher for the reference samples (32.0 kN for ML-I and 28.3 kN for ML-CNT) – Table 4.

All but one ML-I failed in the grips and only one patterned sample failed outside the central region. The patterned samples revealed two different failure modes: in one case the fibre rupture started in CNT patch and propagated instantly through its thickness. In another case, fibre rupture in CNT patch spread over half of its thickness at which point a delamination developed and ran towards the second patch. There it stopped and fibre rupture continued in the second patch though the other half of the sample – Fig. 9. This failure mode resulted in two kinks on the load–displacement curve delaying the ultimate disintegration of the sample. Interestingly the apparent local strength, calculated as the failure load normalised by the thickness at the fibre rupture location, appeared to be noticeably higher for the CNT-enhanced samples: 244 MPa against 224 MPa.

Analysis of surface strain distribution revealed two distinctly different region – in the patch and infused zones – Fig. 8b. Unlike what was seen in the carbon samples, the strain in the patch area was higher than in the infused region – Fig. 8c. There were two counteracting factors that could affect the surface strain distribution and lead to this difference. These were: (a) the contrast in stiffness between the patched and infused areas and (b) the bending effects associated with the thickness variation.

These effects had different impact on the strain in the glass and carbon samples. The bending effects in the carbon panels were more prominent due to greater thickness variation. On the flat side of the sample, where the measurements were taken, compressive strains associated with bending occur in the patch area. These strains are superimposed with the tensile strain resulting in the lower deformation on the patch surface. In contrast, the factors related to the stiffness of matrix, such as the presence of intra-yarn cracks, micro porosity, or nano additives, were more explicit in the glass samples. The impact of the latter became evident from the stiffness degradation trends. In the carbon–epoxy

Table 4
Mechanical properties of tested samples.

Material	5HS-CNT	5HS-P	5HS-I	ML-CNT	ML-I
Load at failure, kN	88.2 ± 4.0	84.4 ± 3.8	104.3 ± 4.7	28.3 ± 0.8	32.0 ± 0.9
Strain at failure, %	0.96 ± 0.03	0.91 ± 0.04	1.10 ± 0.04	1.17 ± 0.03	1.23 ± 0.03
Data normalised with respect to the patch cross-section area					
Young's modulus, GPa	72.0 ± 0.8	71.8 ± 1.1	n/a	20.1 ± 0.4	n/a
Data normalised with respect to the cross-section of infused area					
Young's modulus, GPa	62.1 ± 1.6	61.0 ± 1.6	64.1 ± 0.8	17.8 ± 0.2	17.6 ± 0.3

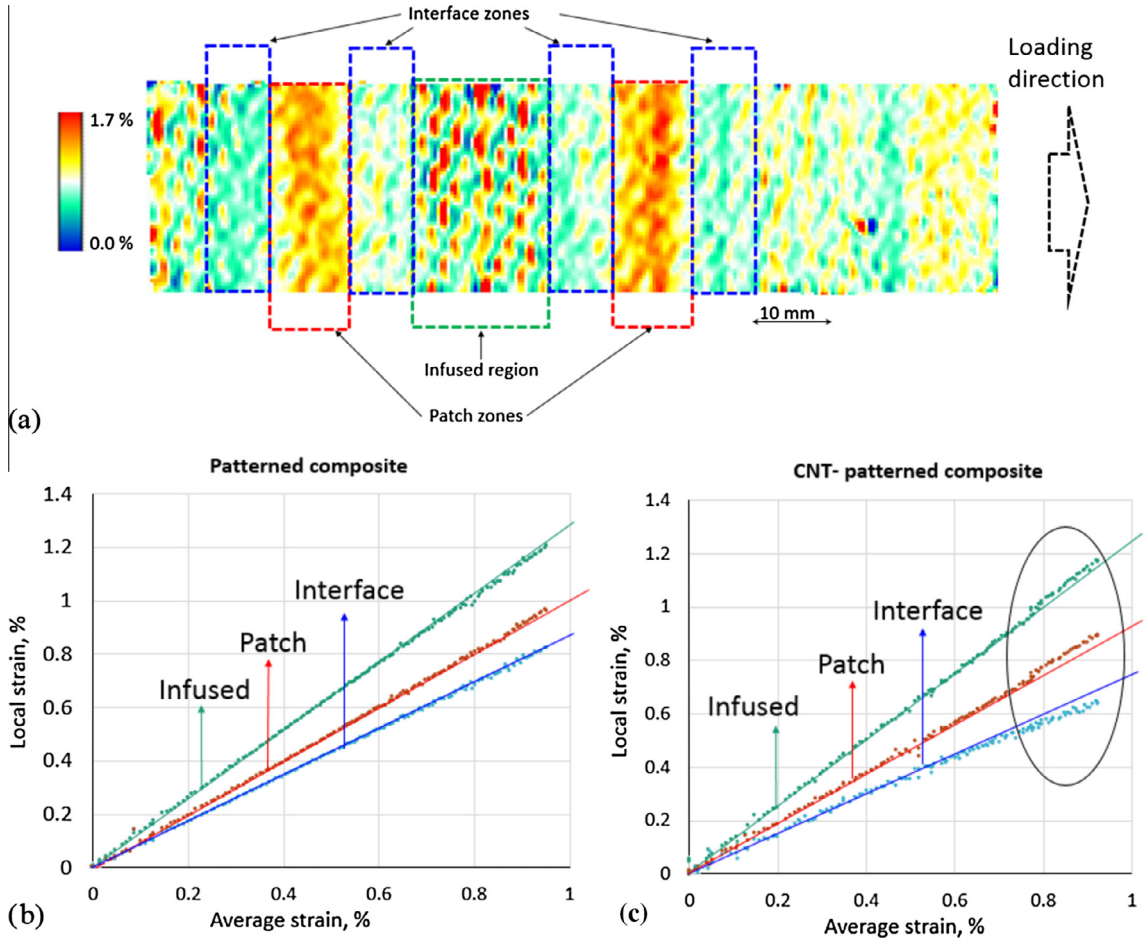

Fig. 7. (a) Characteristic strain distribution in a patterned sample before failure (in loading–horizontal direction), (b) local strain history in the patch, infused and interface areas in composites patterned by Prime 20 resin (b) and CNT enhanced resin, (c) straight solid lines show the trends. Kinks (patched and infused zones) and non-linearity (interface zone) can be seen at ~0.8% in the CNT composite. Straight lines show linear trends and deviations from them. (For interpretation of the references to colour in this figure legend, the reader is referred to the web version of this article.)

systems the material response was dominated by fibres and hence, linear till failure. In the glass–epoxy composites the contribution of non-fibre related factors was more distinct: for instance, intra-yarn damage accumulation led to a prominent reduction in stiffness.

The CNT's on the one hand and pores/cracks on the other hand had competing positive and negative impacts on patch stiffness in the glass samples. The fact that strain was higher in the patch area in the beginning of the test suggested that the porosity could have a larger influence on patch stiffness than the presence of CNT. The evolution of strain provided the insight on damage accumulation. The strain in the infused region remained strictly proportional to the applied strain whereas the rate of strain in the patch region was slowing after ~0.4% of applied strain. A deviation of the strain in the patch from linear trend indicated that damage accumulation was more intense in the infused area.

The optical observation of light transmitted through the sample performed in-situ during the test showed progressive of accumulation of damage seen as white areas on the images – Table 5. The most intensive occurrence of these zones was observed in the transition from patch to infused zones. The damage accumulation was localised as compared to the reference samples which exhibited a uniform evolution of its colour throughout the test.

Micrographs of fractured samples away from the fibre rupture zone revealed different damage patterns in the patches and infused areas – Fig. 10. In the infused areas an intensive intra-yarn cracking was observed reaching up to 2–3 cracks per mm in some yarns. Few local isolated delaminations could also be observed. In the porous transition region, the intensity of micro-cracking was significantly lower, however, frequent intra-yarn in-plane cracks connecting chains of micro pores spanning through the entire yarn were found. These cracks were clearly seen as white areas

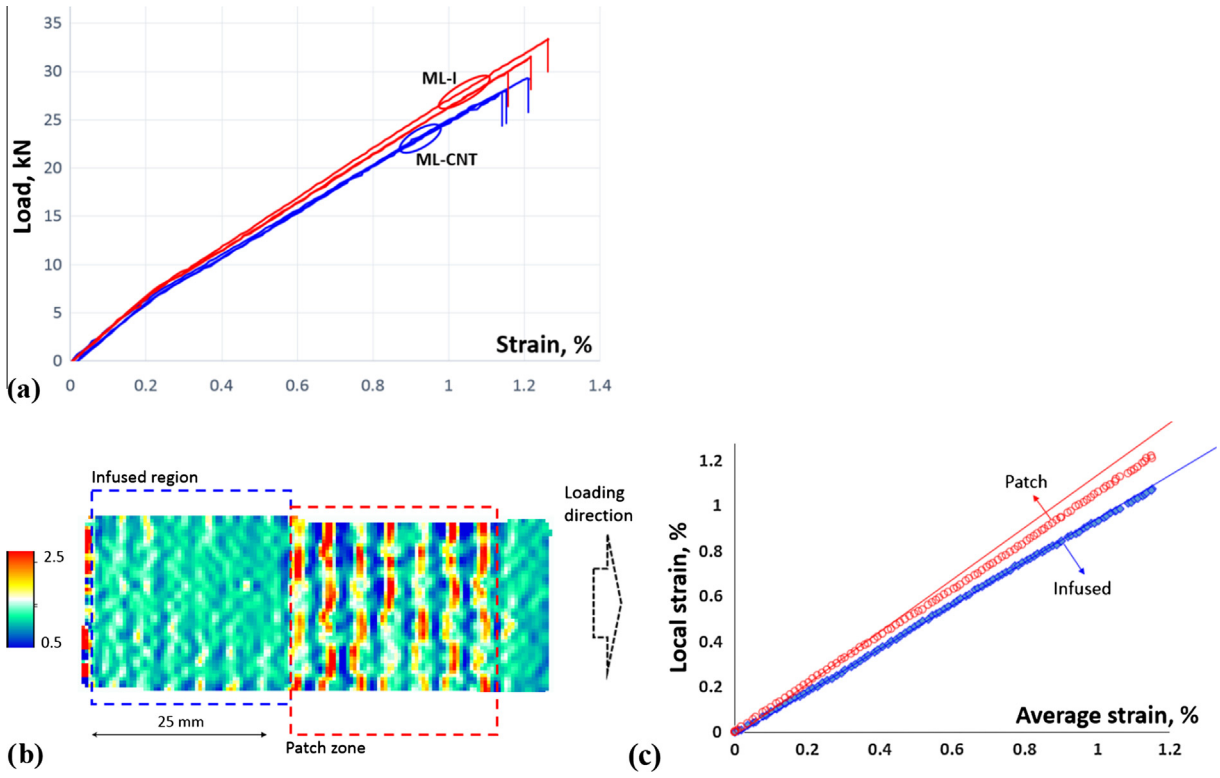

Fig. 8. (a) Mechanical response of the patterned/patched ML-CNT (failed in patch region) and reference ML-I (failed in the grips) samples, (b) characteristic strain distribution in a patterned ML-CNT before failure (in loading–horizontal direction), (c) local strain history in the patch and infused areas in ML composites (straight lines are showing linear trends and a deviation from them). (For interpretation of the references to colour in this figure legend, the reader is referred to the web version of this article.)

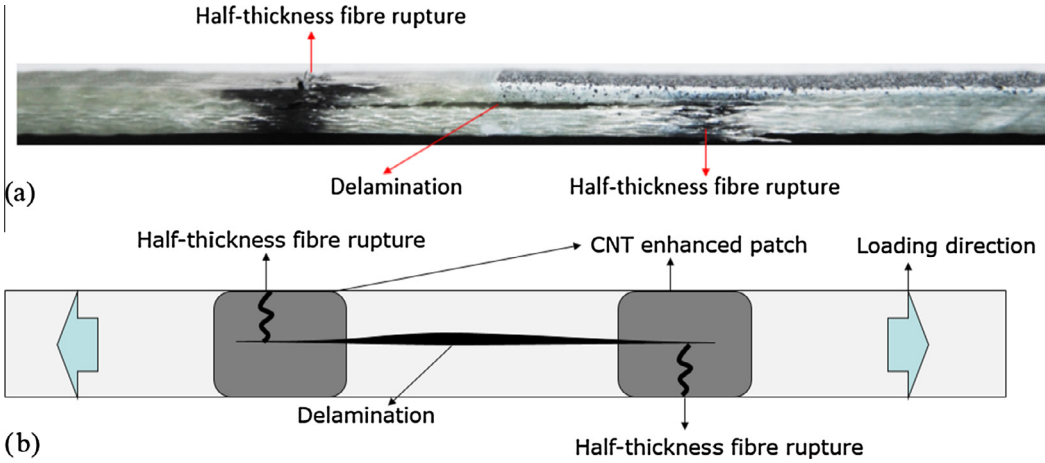

Fig. 9. Side view of glass ML-CNT samples with delamination connecting two patches with half ruptures: (a) sample picture, (b) sketch highlighting the mechanisms of crack development. (For interpretation of the references to colour in this figure legend, the reader is referred to the web version of this article.)

occurring in the transmitted light images at the advanced deformation stages – Table 5. In the patch centre, i.e. CNT rich region, the intensity of intra-yarn cracking was lower (less than 1 crack per mm of a ply). It is interesting to note that this is in agreement with the observations of de Greef et al. [24,25] who found that the presence of CNT hinder the intra-yarn crack density accumulation.

4. Discussion

The tensile test revealed several important features in the behaviour of patterned composites:

(1) The load in tensile test was applied perpendicular to the inter-patch interface, thus revealing the greatest impact that an interface may have on composite properties. Knowing the interface issues in other materials, it could be suggested that breaking integrity of a hypothetical crack-like interface should make a composite more compliant. However, for the considered systems no noticeable effect on stiffness of the patched composite was seen. Only a minor knock-down on secant modulus after failure initiation was detected in glass composites. As evidenced by the micrographs this compliancy was related to higher density of intra-yarn flat cracks in the plane of the composite panel.

(2) An early failure was observed in all the patterned samples which should most likely be attributed to the thickness variation and as a result to additional bending stress occurring in fibres. The patterned material failed systematically in the

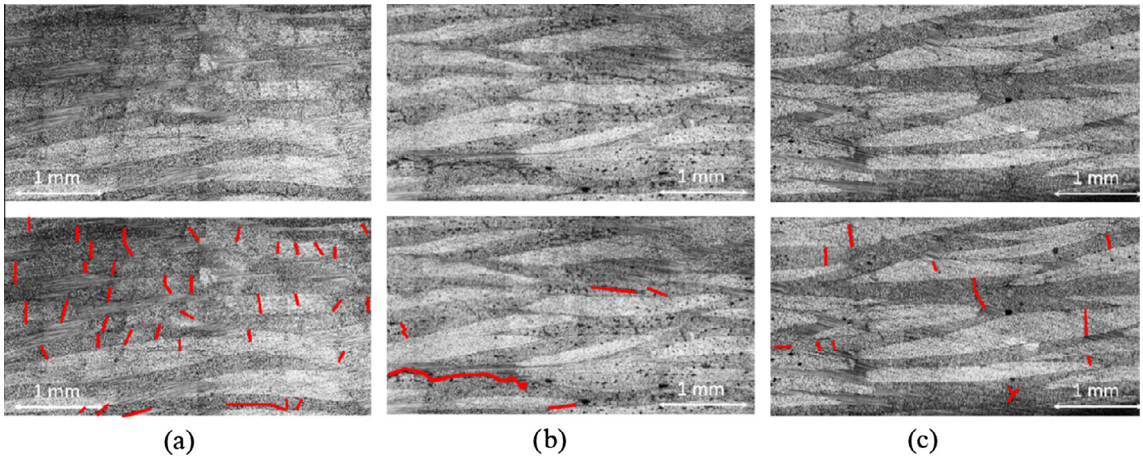

Fig. 10. Representative micrographs of the ML sample brought to failure (cross-sections are at 45° to warp yarns): (a) infused area, (b) transition area, (c) patch centre. Images below highlight crack distribution (in red). (For interpretation of the references to colour in this figure legend, the reader is referred to the web version of this article.)

Table 5
Failure pattern at various levels of strain as seen in the transmitted through thickness light (tensile load is the vertical direction, full width of sample in the horizontal direction is shown, the scale bars shown in left column are applicable to all the images).

Strain, %	0.15	0.35	0.8	1.1
ML-CNT	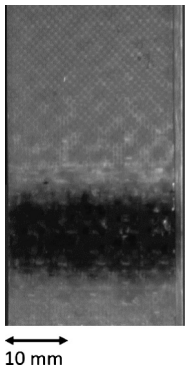	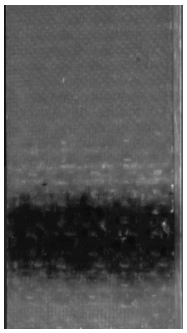	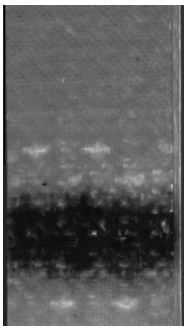	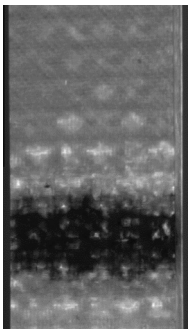
ML-I	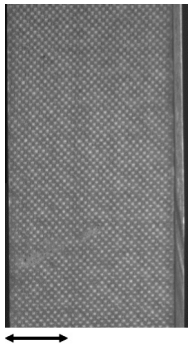	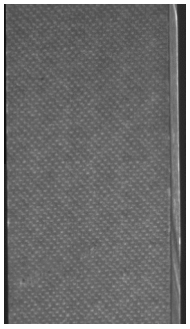	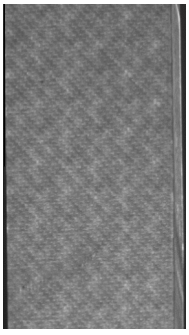	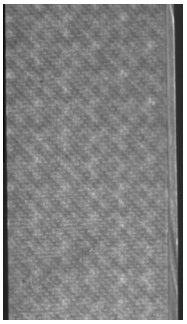

patch or in the interface regions with one sample showing the potential to confine macro delamination in between two rows of patches. Apparently the delamination-like flat cracks, initiated at the interface, triggered the macro-delaminations which propagated instantly between the two patches but was suppressed when entering another patch. This peculiar failure mechanism suggests that patterning may offer a new instrument for manipulating and controlling damage events. However, this failure mode was observed only once and more needs to be done to understand how to control this process consistently.

(3) Surface strain measurement revealed distinctly different regions pointing at various deformation and failure mechanisms in the patterned material. Partially this can be attributed to the waviness of the sample and bending deformation superimposed with the tensile stress. Apart from purely elastic effects, the analysis of the damage pattern in the glass samples indicated different failure mechanisms in the infused (intense intra-yarn matrix cracking), interface (intra-yarn crack in the plane of the sample) and patch areas (low crack density). The patch had both positive and negative effect on crack dynamics. On the one hand, the overall

crack density appeared to be lower in the CNT enhanced region. On the other hand, the patch interface reveals a higher level of porosity which promotes a new type of cracking in that region that can trigger the delamination.

5. Conclusions

A novel method for functionalising and patterning textile composites was demonstrated. It was shown that insulating glass composite can be made electrically conductive. The level of conductivity is drastically higher than what could be achieved by any previous liquid moulding technologies. The major challenges of the functionalization in conventional processes, such as filtering of conductive particles, play to the benefit of the liquid resin print process since the volume fraction of CNT in the injected location increases and hence, a better conductive network can be formed. As opposed to other techniques, the process offers a possibility to add functional properties locally and in any pattern or configuration, which may be defined by requirements to structural or functional performance. This minimises the interference to the subsequent infusion process and reduces the impact of CNT presence on the component performance.

This study showed examples of structures obtained with a novel manufacturing method which exhibited peculiar features: micro-porosity, thickness variation, internal boundaries, non-periodic pattern of the reinforcement, interaction of distinctly different matrices, etc. The impact of these features on the deformation and failure mechanisms was explored. It was found that the material modification had minor effect on the early stages of deformation but may affect (both positively and negatively) the damage accumulation process and the failure of the material. The main negative factor is earlier fibre failure caused by thickness variation. This feature however, as discussed in [1], has a potential of being controlled by organising the structure (e.g. fibre bridging between the patches in quasi-isotropic structures) or modifying manufacturing process (equalising pressure in post-injection consolidation and subsequent liquid moulding process for instance by using rigid mould RTM). Summarising the output of the mechanical testing we can claim that the print process creates a very promising method for creating structural components with added capabilities.

Acknowledgements

The work of Yann LeCahain and Alexandre Dattin was supported by FP7 Marie Curie CIG InterCom project 304062: “New inter-scale techniques for novel composite architectures”. The work of Dmitry Ivanov and Surush Arafati was supported by EPSRC Grant EP/M009149/1: “New generation of manufacturing technologies: liquid print of composite matrices”. The work of Andrey Aniskevich was supported by the Latvian State Research Program “IMATEH”.

References

[1] Ivanov DS, White JAP, Hendry W, Mahadik Y, Minett V, Patel H, et al. Stabilizing textile preforms by means of liquid resin print: a feasibility study. Adv Manuf: Polym Compos Sci 2015;1:26–35.
[2] Thostenson ET, Chou TW. Carbon nanotube networks: sensing of distributed strain and damage for life prediction and self-healing. Adv Mater 2006;18:2837–41.
[3] Starkova O, Mannov E, Schulte K, Aniskevich A. Strain-dependent electrical resistance of epoxy/MWCNT composite after hydrothermal aging. Compos Sci Technol 2015;117:107–13.
[4] Lin Y, Gigliotti M, Lafarie-Frenot MC, Bai J, Marchand D, Mellier D. Experimental study to assess the effect of carbon nanotube addition on the through-thickness electrical conductivity of CFRP laminates for aircraft applications. Compos B 2015;76:31–7.
[5] Gurkan I, Cebeci H. Electrical and mechanical property investigation of fuzzy fibre-reinforced composites. In: Proceedings of 20th International Conference on Composite Materials, Copenhagen 19–24th July 2015.
[6] Zhang J, Zhuang R, Liu JMader, Mader E, Heinrich G, Gao Sh. Functional interphases with multi-walled carbon nanotubes in glass fibre/epoxy composites. Carbon 2010;48:2273–81.
[7] Gao L, Chou T-W, Thostenson ET, Godara A, Zhang Z, Mezzo L. Highly conductive polymer composites based on controlled agglomeration of carbon nanotubes. Carbon 2010;48(9):2649–51.
[8] Herceg T, Greenhalgh E, Bismarck A, Shaffer M. High performance nano and hierarchical composites. In: Proceedings of 20th International Conference on Composite Materials, Copenhagen 19–24th July 2015.
[9] Zhang H, Liu Y, Kuwata M, Bilotti E, Peijs T. Improved fracture toughness and integrated damage sensing capability by spray coated CNTs on carbon fibre prepreg. Composites Part A 2015;70:102–10.
[10] Wichmann MHG, Sumfleth J, Gojny FH, Quaresimin M, Fiedler B, Schulte K. Glass-fibre-reinforced composites with enhanced mechanical and electrical properties – benefits and limitations of a nanoparticle modified matrix. Eng Fract Mech 2006;73:2346–59.
[11] da Costa EFR, Skordos AA, Partridge IK, Rezai A. RTM processing and electrical performance of carbon nanotube modified epoxy/fibre composites. Composites Part A 2012;43:593–602.
[12] Domingues D, Logakis E, Skordos AA. The use of an electric field in the preparation of glass fibre/epoxy composites containing carbon nanotubes. Carbon 2012;50:2493–503.
[13] Böger L, Wichmann M, Meyer L, Schulte K. Load and health monitoring in glass fibre reinforced composites with an electrically conductive nanocomposite epoxy matrix. Compos Sci Technol 2008;68(7–8):1886–94.
[14] Thostenson ET, Gangloff JJ, Li CY, Byun JH. Electrical anisotropy in multiscale nanotube/fiber hybrid composites. Appl Phys Lett 2009;95(7). 073111-1-3.
[15] Lomov SV, Gorbatokh L, Houlle M, Kotanjac Z, Koissin V, Vallons K, et al. Compression resistance and hysteresis of carbon fibre tows with grown carbon nanotubes/nanofibers. Compos Sci Technol 2011;71:1746–53.
[16] Aravand M, Lomov SV, Verpoest I, Gorbatikh L. Evolution of carbon nanotube dispersion in preparation of epoxy-based composites: from a masterbatch to a nanocomposite. Express Polym. Lett. 2014;8(8):596–608.
[17] Verpoest I, Lomov SV. Virtual textile composites software Wisetex: integration with micro-mechanical, permeability and structural analysis. Compos Sci Technol 2005;65(15–16):2563–74.
[18] Korayem AH, Barati MR, Simon GP, Zhao XL, Duan WH. Reinforcing brittle and ductile epoxy matrices using carbon nanotubes masterbatch. Compos A 2014;61:126–33.
[19] Fan Z, Hsiao K-T, Advani SG. Experimental investigation of dispersion during flow of multi-walled carbon nanotube/polymer suspension in fibrous porous media. Carbon 2004;42:871–6.
[20] Todoroki A, Tanaka M, Shimamura Y. Measurement of orthotropic electric conductance of CFRP laminates and analysis of the effect on delamination monitoring with an electric resistance change method. J Compos Sci Technol 2002;62:619–28.
[21] Ma C, Zhang W, Zhu Y, Ji L, Zhang R, Koratkar N. Alignment and dispersion of functionalized carbon nanotubes in polymer composites induced by an electric field. Carbon 2008;46(4):706–20.
[22] Domingues D, Logakis E, Skordos AA. The use of an electric field in the preparation of glass fibre/epoxy composites containing carbon nano-tubes. Carbon 2012;50:2493–503.
[23] Choi ES, Brooks JS, Eaton DL, Al-Haik MS, Hussaini MY, Garmestani H. Enhancement of thermal and electrical properties of carbon nanotube polymer composites by magnetic field processing. J Appl Phys 2003;94(9):6034–9.
[24] De Greef N, Gorbatikh L, Godara A, Mezzo L, Lomov SV, Verpoest I. The effect of carbon nanotubes on the damage development in carbon fiber/epoxy composites. Carbon 2011;49(14):4650–64.
[25] De Greef N, Gorbatikh L, Lomov SV, Verpoest I. Damage development in woven carbon fiber/epoxy composites modified with carbon nanotubes under tension in the bias direction. Compos A 2011;42(11):1635–44.